Journal of
Nanoscience and Nanotechnology
Vol. 7, 1043–1051, 2007

Mean Magnetic Moment of Polydisperse Superparamagnetic Nanoparticles: Correlation Between Grain Size and Magnetic Moment Distributions

J. S. Blázquez, V. Franco, C. F. Conde, and A. Conde*

Departamento de Física de la Materia Condensada, ICMSE-CSIC, Universidad de Sevilla, P. O. Box 1065, 41080 Sevilla, Spain

The field dependence of magnetization in superparamagnetic systems can be fitted using a set of Langevin contributions characterized by their particle densities and their magnetic moments. In fact, these contributions are just partial average values over the actual magnetic moment distribution of the system. The achievement of the most adequate mean magnetic moment is non-trivial and depends on the characteristics of the moment distribution and the applied magnetic field range. As an example, results have been applied to a nanocrystalline alloy.

Keywords: Nanocrystalline Alloys, Soft Magnets, Nanocrystalline Microstructure, Superparamagnetism.

1. INTRODUCTION

From technological and fundamental points of view, nanostructured materials are a field of intensive research. The high percentage of atoms located at the surface of the crystallites can produce strong differences between the properties (mechanical, magnetic, etc.) of nanostructured systems and their bulk counterparts.[1] Particularly, Fe-based nanocrystalline alloys show outstanding properties for soft magnetic applications.[2] The responsible for this extreme softness is the two phase character of these systems: nano-sized ferromagnetic crystallites embedded in a residual amorphous matrix, also ferromagnetic but with a lower Curie temperature. This configuration yields an averaging out of the magnetocrystalline anisotropy due to the exchange coupling between nanocrystals at temperatures below the Curie temperature of the amorphous phase.[3] Above this temperature, the amorphous matrix becomes paramagnetic and, at high enough temperatures, the crystallites could behave as isolated superparamagnetic particles,[4,5] provided that the dipolar interactions between them are negligible.[6,7]

The field and thermal dependence of magnetization, M, of a set of identical superparamagnetic particles is described by:

$$M = N\mu L\left(\frac{\mu H}{kT}\right) \quad (1)$$

where N is the number density of the particles, μ is the magnetic moment of the individual particles, L is the Langevin function, H is the applied magnetic field, k is the Boltzmann constant, and T is the temperature. However, real samples rarely show a unique grain size but a distribution of grain sizes and, consequently, a distribution of magnetic moments. The determination of grain size distributions for this sort of samples is usually performed by transmission electron microscopy. However, the comparison with results on grain size distributions obtained by other techniques is still a subject of current interest.[8–11]

From the magnetic point of view, the grain size distribution is evidenced by a magnetic moment distribution. Therefore, the magnetic response of such complex superparamagnetic materials might be fitted with the help of several contributions.[12–15] Although there are numerical methods to extract a quasicontinuous moment distribution from the magnetization curves,[15–18] the increase of free fitting parameters can prevent a direct physical interpretation of the results. Therefore, a compromise must be reached to describe the behaviour of the real system with the less possible number of free parameters. Changing from a continuous to a discrete description implies that, for each particular physical magnitude, the continuous distribution of its values is grouped in partial average values. The simplest discrete representation of the system would be to use a mean value to describe the whole system.

*Author to whom correspondence should be addressed.

Different definitions of average magnetic moment: The transition from a continuous system to its discrete description has to be made in the most accurate way. Therefore, although there are different definitions of average magnetic moments currently used in the literature, the adequacy of each of them for accurately describing an underlying experimental system has to be tested. Although there is no strict argument to *a priori* select any particular definition of the average moment, a result of this study will suggest the conditions under which they are the most reliable ones.

The most straightforward definition of the average magnetic moment is to base it on the number density of the particles with different magnetic moments (e.g. Refs. [19, 20]):

$$\langle \mu_N \rangle = \frac{\sum N_i \mu_i}{\sum N_i} \tag{2}$$

In other cases, for the calculation of $\langle \mu \rangle$ the magnetic moment of the particles is weighted with their contribution to the overall magnetization ($M_i = N_i \mu_i$) (e.g. Refs. [7, 12]):

$$\langle \mu_M \rangle = \frac{\sum M_i \mu_i}{\sum M_i} = \frac{\sum N_i \mu_i^2}{\sum N_i \mu_i} \tag{3}$$

The physical meaning of this second definition can be clarified by considering an ideal system composed of identical atoms, with magnetic moment μ_{at}. The magnetic moment of a particle composed of n_i atoms is $\mu_i = n_i \mu_{at}$ and, from Eq. (3), $\langle \mu_M \rangle$ would be:

$$\langle \mu_M \rangle = \frac{\sum N_i n_i \mu_i}{\sum N_i n_i} \tag{4}$$

Therefore, while the first definition, $\langle \mu_N \rangle$, takes into account the number of particles with magnetic moment μ_i, the second one, $\langle \mu_M \rangle$, considers the number of atoms in each particle with magnetic moment μ_i and hence, the weight factor for calculating the average moment is $N_i n_i$. Whereas $\langle \mu_N \rangle$ has an intensive nature, in the sense that all particles contribute equally to the average moment, $\langle \mu_M \rangle$ is extensive, as the contribution of each moment emerges from the number of atoms in the particles.

In fact, analogous situation can be found in nonmagnetic problems when describing the properties of particulate systems in terms of mean values. For example, in TEM images, average grain size determination is usually performed by counting the particles with a specific size and making the numerical average. Therefore, all the particles, big or small, contribute equally to the average value, as for $\langle \mu_N \rangle$. However, when mean grain size is estimated from the broadening of the diffraction maximum, each particle contributes to the diffracted intensity of a maximum with a width related to its size, dependent on the number of atoms which form that particle. As larger particles yield higher intensity peaks, they contribute more to the total intensity. This situation is analogous to that of $\langle \mu_M \rangle$.

Different criteria of selection of the most adequate average magnetic moment: In order to choose the most representative mean value describing a system it is necessary to establish some selection criteria. One criterion to determine the most adequate $\langle \mu \rangle$ to be used would be to find that which better represents the magnetization curve of the polydisperse system of interest. Another criterion would be to find that moment which better makes the reduced magnetization curves collapse when represented as a function of $\langle \mu \rangle H/kT$.

The aim of this work is to test the adequacy of the two proposed mean magnetic moments according to the two defined criteria. This will be done from the analysis of the magnetization curves of a superparamagnetic system. As an application, results will be correlated with those of other techniques such as differential scanning calorimetry, DSC, and transmission electron microscopy, TEM, for the same system.

This paper is structured in the following sections. After this introduction, in the second section, the influence of the characteristics of the magnetic moment distribution on the adequacy of the two proposed methods of calculating $\langle \mu \rangle$ ($\langle \mu_N \rangle$ and $\langle \mu_M \rangle$) is analyzed with the help of numerically generated magnetization curves. In the third section, an application of the previous numerical results to a real case is made. A nanocrystalline alloy ($Fe_{68.5}Mo_5Si_{13.5}B_9Cu_1Nb_3$) has been chosen because both mean magnetic moment definitions are commonly employed in the literature for this kind of system. Finally, the main conclusions achieved in this study are summarized.

2. INFLUENCE OF THE MAGNETIC MOMENT DISTRIBUTION ON THE CALCULATION OF $\langle \mu \rangle$

The aim of this section is to identify which of the two definitions of mean magnetic moment is the most adequate to describe ideal polydisperse systems. Using numerically generated curves, the uncertainties which could arise from the sample preparation and/or characterization techniques can be avoided.

The magnetization of a quasicontinuous magnetic moment distribution could be generated as the starting point for the analysis. However, the large number of parameters involved could jeopardize the physical meaning of the results regarding $\langle \mu \rangle$. Therefore, the more simplistic approach of considering only two contributions has been used in this study:

$$M = N_1 \mu_1 L\left(\frac{\mu_1 H}{kT}\right) + N_2 \mu_2 L\left(\frac{\mu_2 H}{kT}\right) \tag{5}$$

where M is the magnetization of the system, N_1 and N_2 are the particle densities, and μ_1 and μ_2 are the corresponding magnetic moments. This simple magnetic moment distribution can be characterized by the ratios between its two magnetic moments and its two particle densities (μ_2/μ_1 and N_2/N_1, respectively). The M curves were generated in a μ_2/μ_1 range from 0 to 1 with a step of 0.05. Regarding

the N_2/N_1 ratio, three different values (1, 5, and 10) have been considered. This choice is justified by the typical TEM results for nanocrystalline alloys. An example is given in Section 3, showing asymmetrical grain size distributions in which the amount of small particles is enhanced. This selection of two fitting moments does not imply an assumption of a bimodal distribution of the real samples. In fact, a continuous distribution can be represented with big enough "bins" as that of two adding contributions. This low resolution in bin selection emerges from the ill-posed nature of the problem: the extraction of a moment distribution from the fitting of the global magnetic response of the sample, where the physical meaning of the fitting parameters is progressively lost as their number increases.

2.1. $\langle\mu\rangle$ from the Best Fit of the Magnetization Curve to a Monodisperse System

In order to identify the most adequate mean magnetic moment following the first criterion (the monodisperse system which better substitutes the polydisperse one), each of the generated magnetization curves (with different values of μ_2/μ_1 and N_2/N_1) were fitted to:

$$M = N_{\mathrm{FIT}}\mu_{\mathrm{FIT}}L\left(\frac{\mu_{\mathrm{FIT}}H}{kT}\right) \tag{6}$$

where μ_{FIT} is the magnetic moment and N_{FIT} is the particle density obtained from each fitting.

The values of $\langle\mu_N\rangle$ (numerical average value of magnetic moments of the system) and $\langle\mu_M\rangle$ (average value weighted with the individual magnetization of each particle type), corresponding to each generated magnetic moment distribution were also obtained. The comparison between these two mean values and μ_{FIT} yields the selection of the most adequate method to calculate $\langle\mu\rangle$. As an example, Figure 1(a) shows μ_{FIT}, $\langle\mu_N\rangle$ and $\langle\mu_M\rangle$ dependence on the μ_2/μ_1 ratio for $N_2/N_1 = 5$, the behaviour for the other particle density ratios being similar. Figure 1(b) shows the absolute values of the differences $\Delta_N = |\mu_{\mathrm{FIT}} - \langle\mu_N\rangle|$ and $\Delta_M = |\mu_{\mathrm{FIT}} - \langle\mu_M\rangle|$ as a function of μ_2/μ_1 ratio for the three studied values of N_2/N_1 (1, 5, and 10). Although the general trend of μ_{FIT} is more similar to that of $\langle\mu_M\rangle$, there are regions where Δ_N is smaller than Δ_M. Therefore, according to this criterion, the identification of the most representative mean magnetic moment (in the sense that the magnetization curve of this single moment can substitute the generated one) depends on the characteristics of the moment distribution. For example, for small μ_2/μ_1 (i.e., broad particle size distributions) $\langle\mu_M\rangle$ should be selected.

Regarding the particle densities, as the saturation magnetization of the system, M_S, should be independent of the average magnetic moment selected to represent the system, the following relationship must be fulfilled:

$$M_S = \sum N_i\mu_i = N^*\langle\mu\rangle \tag{7}$$

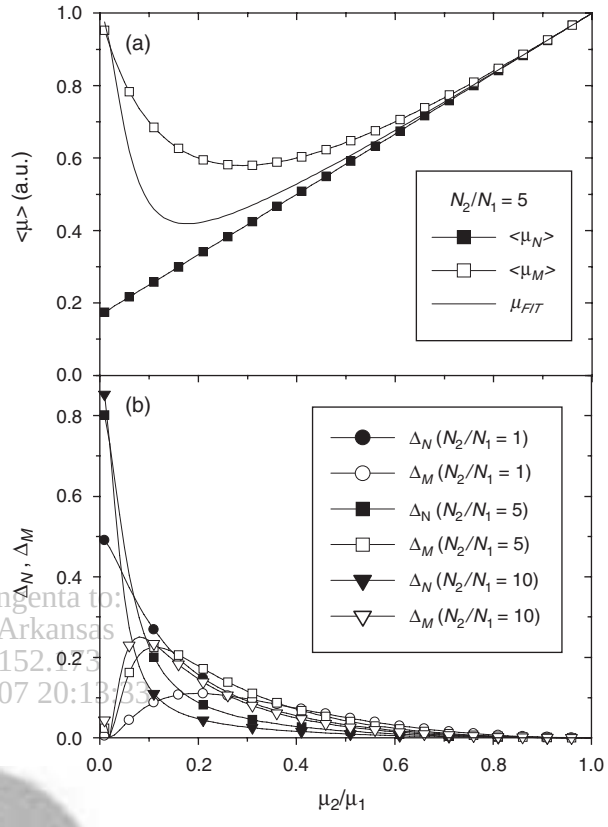

Fig. 1. (a) Normalized magnetic moment of the generated magnetization curve μ_{FIT} and calculated average values, $\langle\mu_M\rangle$ and $\langle\mu_N\rangle$, as a function of μ_2/μ_1 for $N_2/N_1 = 5$. (b) Absolute values of the difference between both average values and μ_{FIT}.

where N^* is the effective particle density (N_N^* or N_M^*) and $\langle\mu\rangle$ is the corresponding average value of the magnetic moment ($\langle\mu_N\rangle$ or $\langle\mu_M\rangle$). Introducing the definitions of $\langle\mu_N\rangle$ and $\langle\mu_M\rangle$ (Eqs. (2) and (3), respectively) inside Eq. (7), it can be shown that N_N^* is equal to the actual particle density $N_N^* = N_1 + N_2$. However, in the case of $\langle\mu_M\rangle$ the effective population density is:

$$N_M^* = \frac{(N_1\mu_1 + N_2\mu_2)^2}{N_1\mu_1^2 + N_2\mu_2^2} \tag{8}$$

It is worth noticing that N_M^* is analogous to other effective densities as it occurs with the effective density involved in the Hall effect of a system with two different types of carriers.

As an example, Figure 2 shows the dependence of N_N^*, N_M^*, and N_{FIT} and the relative differences $\delta_N = |N_{\mathrm{FIT}} - N_N^*|/(N_1 + N_2)$ and $\delta_M = |N_{\mathrm{FIT}} - N_M^*|/(N_1 + N_2)$ on μ_2/μ_1 for $N_2/N_1 = 5$. Similar behaviour could be observed for the other particle density ratios. As expected, the general trend is also better represented by N_M^* than by N_N^*. However, for high values of μ_2/μ_1, the error between the fitting and the calculated values is smaller when N_N^* is considered. In all cases, the region where $\delta_N < \delta_M$ is included in the region where $\Delta_N < \Delta_M$ but they are not exactly coincident. It must be taken into account that the N^* value was

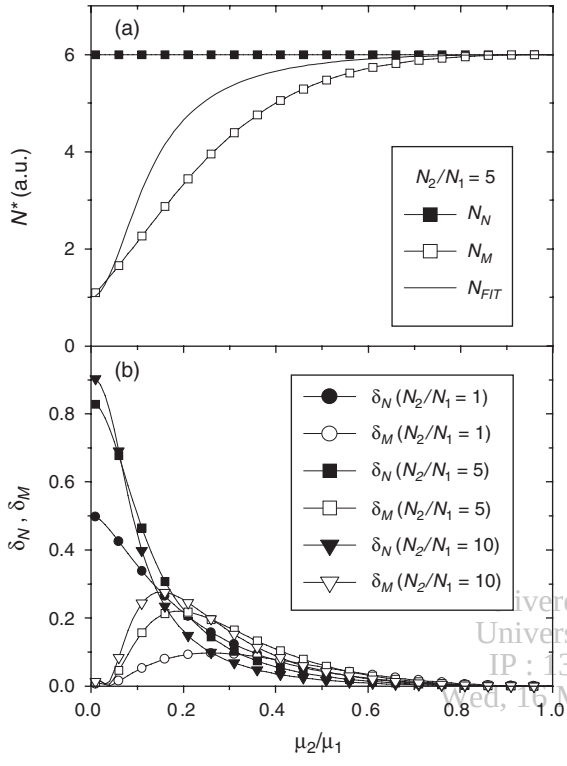

Fig. 2. (a) Particle density of the generated magnetization curve N_{FIT} and calculated effective values, N_M and N_N, as a function of μ_2/μ_1. (b) Absolute values of the difference between both effective values and N_{FIT}.

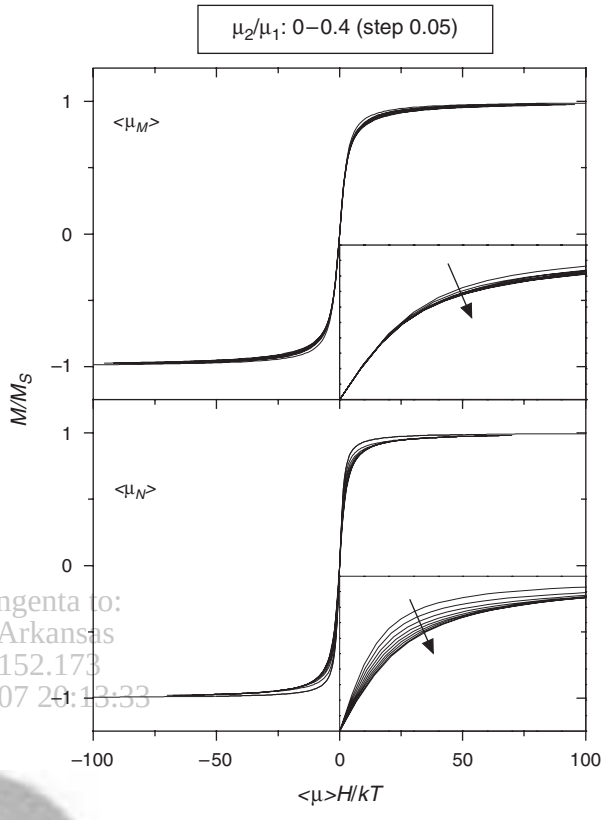

Fig. 3. Generated magnetization curves after rescaling in a range of μ_2/μ_1 from 0 to 0.4 for $N_2/N_1 = 1$, using $\langle\mu_M\rangle$ (above) and $\langle\mu_N\rangle$ (below). The inset shows an enlargement (10 times in the x axis) of the low field region of the curves. The arrow indicates the increasing trend of μ_2/μ_1.

just calculated imposing that the saturation magnetization of the system remains constant regardless of the selection of $\langle\mu\rangle$ (Eq. (7)).

2.2. $\langle\mu\rangle$ from the Collapse of Magnetization Curves After Rescaling

Following the second criterion, the way to determine the most adequate mean magnetic moment is to find the $\langle\mu\rangle$ which makes the reduced magnetization (M/M_S) curves collapse when represented as a function of $\langle\mu\rangle H/kT$. This rescaled x axis is related to the ratio between the average magnetic energy of a system with a distribution of magnetic moments and its thermal energy.

Analogously to the previous subsection, the two previously defined mean magnetic moments $\langle\mu_N\rangle$ and $\langle\mu_M\rangle$ can be used to rescale the generated M curves. Figure 3 shows the generated magnetization curves after rescaling in a range of μ_2/μ_1 from 0 to 0.4 for $N_2/N_1 = 1$. It can be observed that in this range the collapse obtained from $\langle\mu_M\rangle$ is better than the one from $\langle\mu_N\rangle$. Figure 4 shows the generated magnetization curves after rescaling in a range of μ_2/μ_1 from 0.4 to 1 for $N_2/N_1 = 1$. Unlike the results of Figure 3, in this case it is clear that the collapsing of the curves using $\langle\mu_N\rangle$ is much better than the one using $\langle\mu_M\rangle$. From this feature, it is evident that as the distribution becomes narrower (μ_2/μ_1 tends to 1) $\langle\mu_N\rangle$ should be used. However, for small values of μ_2/μ_1, $\langle\mu_M\rangle$ is roughly better. Nevertheless, for different values of N_2/N_1, the selection of $\langle\mu\rangle$ can change, although the general trend is maintained. These results are in agreement with those obtained by the first selection criterion (Section 2.1).

3. APPLICATION TO A REAL SUPERPARAMAGNETIC SYSTEM: $Fe_{68.5}Mo_5Si_{13.5}B_9Cu_1Nb_3$ NANOCRYSTALLINE ALLOY

Ribbons of $Fe_{68.5}Mo_5Si_{13.5}B_9Cu_1Nb_3$ alloy (~25 μm thick and ~10 mm wide) were produced by planar flow casting. Figure 5 shows the differential scanning calorimetry (DSC) plot of the as-quenched alloy, measured in a Perkin-Elmer DSC-7. Devitrification occurs in two stages, the first one corresponds to the formation of nanocrystals of a α-Fe(Si) phase embedded in a residual amorphous matrix and the second one yields the fully crystallization of the material after the formation of boride phases.[21] Transmission electron microscopy (TEM) observations of the samples were performed in a Philips CM200 electron microscope (200 kV). The field dependence of the magnetization curves, measured at different temperatures, was registered in a Lakeshore 7407 Vibrating Sample Magnetometer (VSM) equipped with a furnace, using a maximum applied field of 5 kOe. In order to develop different nanocrystalline microstructure, as-quenched samples

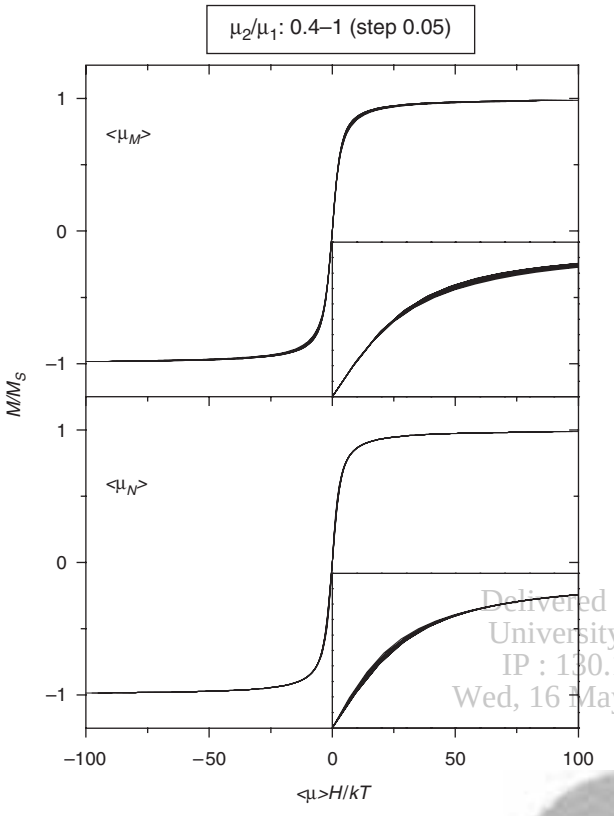

Fig. 4. Generated magnetization curves after rescaling in a range of μ_2/μ_1 from 0.4 to 1 for $N_2/N_1 = 1$, using $\langle\mu_M\rangle$ (above) and $\langle\mu_N\rangle$ (below). The inset shows an enlargement (10 times in the x axis) of the low field region of the curves.

were heated up to different temperatures, T_a (in the range 843–883 K, see Fig. 5), at 10 K/min, in a halogen-lamp furnace under vacuum, and subsequent free cooling.

3.1. Magnetization Results

The temperature dependence of coercivity (Fig. 6) can be explained on the basis of the random anisotropy model

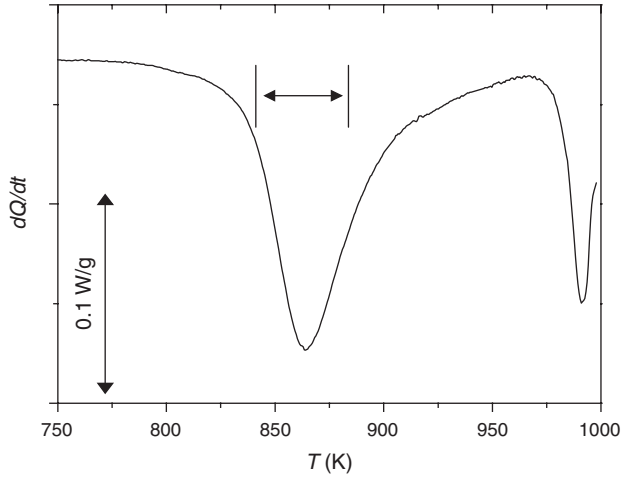

Fig. 5. DSC plot at 10 K/min of as-quenched sample. Lines indicate the T_a range.

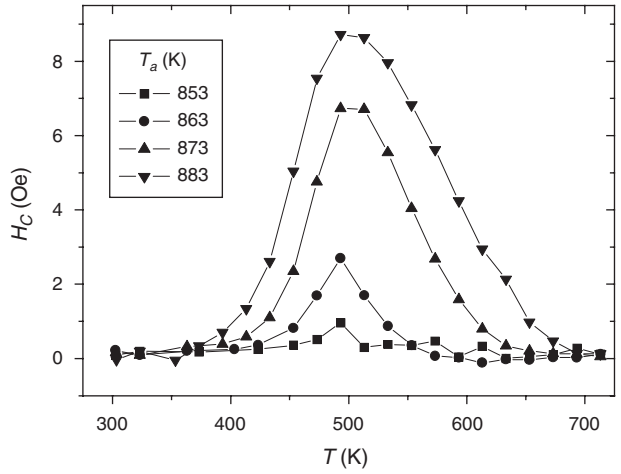

Fig. 6. Temperature dependence of the coercivity. Data for the sample pre-heated up to 843 K are below the field sensitivity of the system.

extended to two-phase systems.[3] For $T < T_c^{am}$ (about 500 K) the ferromagnetic character of the matrix facilitates the exchange coupling of the nanocrystals, resulting in the averaging out of the magnetic anisotropy. As T_c^{am} is approached, the matrix can no longer transmit the exchange. This is evidenced by the progressive increase in coercivity. The reduction in coercivity at higher temperatures is associated to the transition to a superparamagnetic regime of the α-Fe(Si) nanoparticles. It has been shown that this transition is controlled by the dipolar interaction between the particles, both in Finemet[6] and Nanoperm[7] type nanocrystalline materials. The maximum value of coercivity is related to the effective dipolar interaction field. As nanocrystallization proceeds, the increase in grain size and the reduction of the average distance between the nanocrystals enhance the dipolar coupling between the particles, as evidenced by the progressive increase in the maximum value of coercivity. For $T = 713$ K, all the samples present zero coercivity due to the superparamagnetic behaviour of the nanocrystalline system. The $M(H)$ curves registered at this temperature were fitted using two Langevin contributions as well as a lineal term which accounts for the contributions to $M(H)$ from the amorphous matrix and the sample holder (Fig. 7 shows an example). Table I summarizes the fitting results as well as the corresponding calculated $\langle\mu_N\rangle$ and $\langle\mu_M\rangle$ values.

Following the first criterion (Section 2.1), the experimental magnetization curves, after subtraction of the linear term, are compared to the resulting curves using $\langle\mu_N\rangle$ and $\langle\mu_M\rangle$ corresponding to the values obtained from the previously mentioned fittings (Fig. 8 shows an example of the typical behaviour). It is observed that the experimental curve is more similar to that obtained from $\langle\mu_N\rangle$ in all the studied cases. It is worth noticing that for very low magnetic fields (<100 Oe) the use of $\langle\mu_M\rangle$ is better than the use of $\langle\mu_N\rangle$ as it can be observed in the inset of Figure 8. This is in agreement with the fact that in the calculation of $\langle\mu_M\rangle$ the contribution of the larger particles,

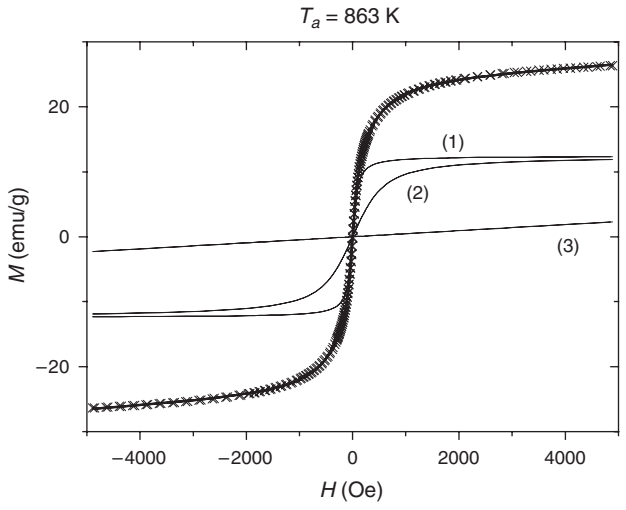

Fig. 7. Experimental $M(H)$ curve at 713 K of nanocrystalline sample pre-heated up to 863 K (crosses) along with the resulting curve of the fit and the different contributions used: two Langevin functions, (1) and (2), and a linear term (3).

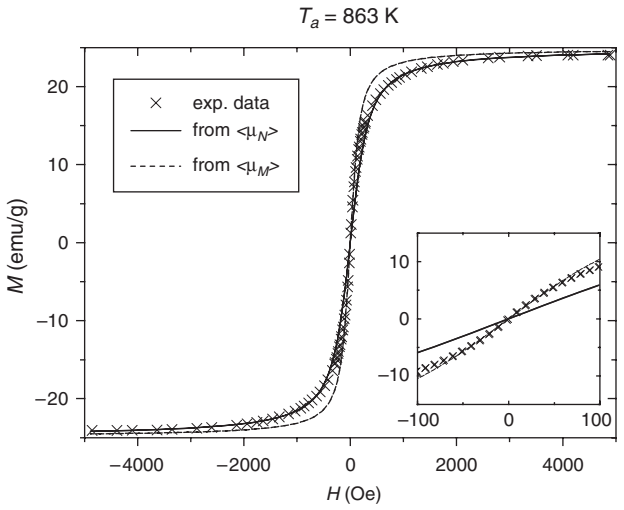

Fig. 8. Experimental $M(H)$ curve at 713 K of nanocrystalline sample pre-heated up to 863 K along with the calculated $M(H)$ curves corresponding to the two different mean magnetic moments: $\langle\mu_M\rangle$ and $\langle\mu_N\rangle$. An enlargement of the figure in the low field region is shown as an inset.

which are responsible for the big slope at low fields, is enhanced. On the other hand, the slowly saturating evolution of $M(H)$ at high fields is mainly due to the smaller particles, which are better taken into account by $\langle\mu_N\rangle$. In fact, for all the studied samples, the values of N_2/N_1 range from 5.5 to 8.4 and μ_2/μ_1 from 0.10 to 0.32, respectively, and, as these values lay on the region where $\Delta_N < \Delta_M$, the experimental magnetization curves can be better represented by $\langle\mu_N\rangle$, in agreement with the results obtained in Section 2.1.

Following the second criterion (Section 2.2), the x axis is rescaled using both possible mean magnetic moments (Fig. 9). It can be observed that using $\langle\mu_N\rangle$ the collapse is better fulfilled than using $\langle\mu_M\rangle$, in agreement with the results obtained above.

3.2. TEM Results

Figure 10 shows bright field (BF) TEM images of the studied samples, their corresponding selected area diffraction (SAD) patterns are included as insets (diameter of the selected area ~0.5 μm). For all the samples, nanocrystalline microstructure (α-Fe(Si) phase embedded in residual amorphous matrix) can be observed, in agreement with SAD patterns. The amount of α-Fe(Si) crystalline phase increases as T_a increases, as it could be expected from DSC results.

The shape of the nanocrystals is approximately spheroidal, characteristic of FINEMET-type alloys, unlike the irregular shaped crystals observed for Cu-free NANOPERM alloys.[2, 22]

Grain size distributions, $n(D)$, were obtained from BF images. Figure 11 shows the $n(D)$ histograms for all the studied samples. It can be observed a continuous increase of the fraction of crystallites exceeding 10 nm, while that of the crystallites below 5 nm decreases. The average grain size $\langle D\rangle$ continuously increases from 6 up to 10 nm. It is evident that the grain size distributions of the studied samples are not bimodal. However, the use of only two components simplifies enormously the description of the system but keeping some relevant information, as the asymmetry of the distribution.

3.3. Comparison Between DSC, TEM, and VSM Results

The progress of the nanocrystallization can be followed from the results of the three characterization techniques (DSC, TEM, and VSM) used in this study. In the case of DSC results, the enthalpy change rate, *dQ/dt*, can

Table I. Parameters from the fit of the $M(H)$ curves of nanocrystalline samples at 713 K. Average values are also shown.

T_a K	μ_1 10^{-16} emu	μ_2 10^{-16} emu	N_1 10^{15} g^{-1}	N_2 10^{15} g^{-1}	$\langle\mu_N\rangle$ 10^{-16} emu	$\langle\mu_M\rangle$ 10^{-16} emu	N_N 10^{15} g^{-1}	N_M 10^{15} g^{-1}
843	8.1	2.6	1.9	15.7	3.2	4.1	17.6	13.7
853	13.8	3.0	4.5	30.5	4.4	7.4	35.0	21.0
863	23.8	4.3	5.2	28.8	7.3	14.0	34.0	17.7
873	43.7	6.3	4.1	26.8	11.2	25.4	30.9	13.6
883	87.4	8.4	2.5	20.7	17.1	52.7	23.2	7.5

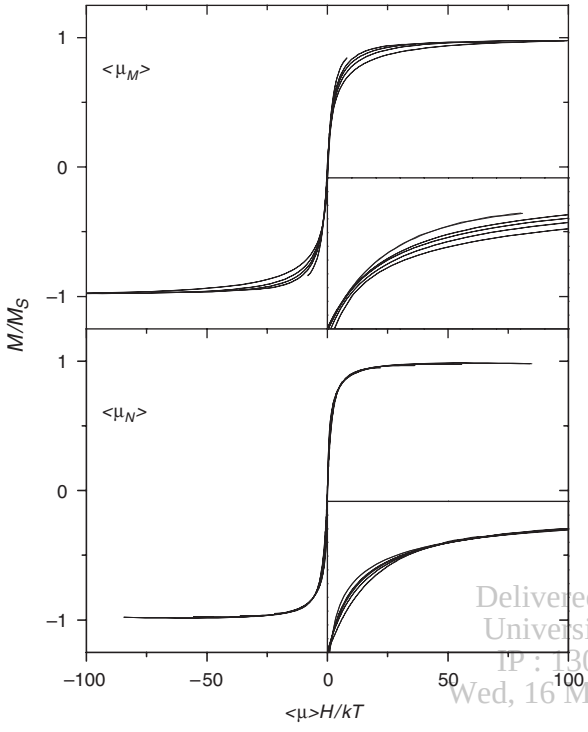

Fig. 9. Rescaled plot of the different experimental $M(H)$ curves obtained at 713 K for the different studied samples using $\langle\mu_M\rangle$ (above) and $\langle\mu_N\rangle$ (below). The insets show an enlargement (10 times in the x axis) of the low field region of the curves.

be assumed proportional to the transformation change. This approximation is less adequate at the end of the transformation[23] but in the studied case samples are heated up to ∼100 K below the end of the nanocrystallization process (see Fig. 5). Therefore, the crystallization fraction can be obtained from the integration of the DSC signal from the onset temperature up to T_a normalized to the total area of the nanocrystallization peak, ΔQ.

$$X_C^{\mathrm{DSC}} = \frac{1}{\Delta Q}\int_{T_{\mathrm{onset}}}^{T_{\mathrm{heat}}} \frac{1}{\beta}\frac{dQ}{dt}dT \tag{9}$$

where β is the heating rate.

It must be taken into account that X_C^{DSC} (fraction of nanocrystallization process) is not the crystalline volume fraction, because at the end of the nanocrystallization process some amount of residual amorphous remains, which will be transformed during the second transformation stage.

In the case of TEM, if a set of images obtained in the same conditions are compared, the crystalline volume (measured after the addition of the volumes of each crystal, V_i, for a statistically significant number of them) is proportional to the crystalline volume fraction of the system.

$$X_C^{\mathrm{TEM}} = A\sum_i V_i \tag{10}$$

where A is a constant. In order to accept this assertion, it must be assumed that the explored volume in each BF TEM image is constant, which implies that the thickness of the observed regions is the same for all the studied samples.

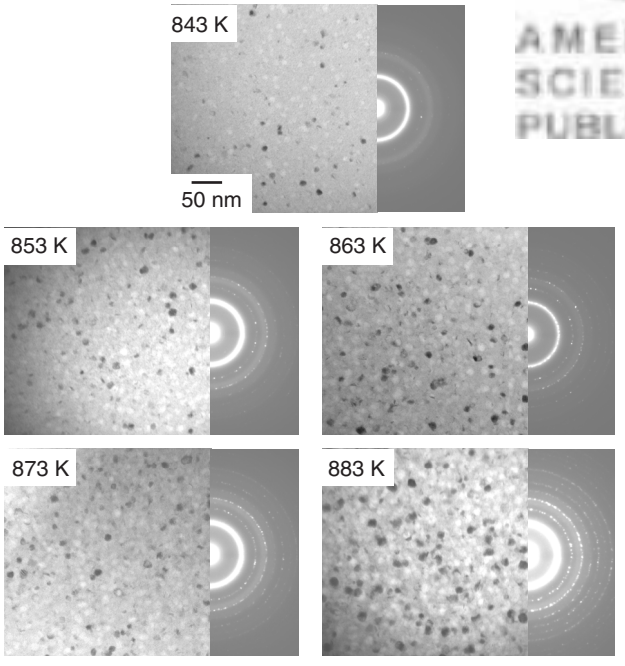

Fig. 10. Bright field images and selected area diffraction patterns of nanocrystalline samples pre-heated up to different T_a.

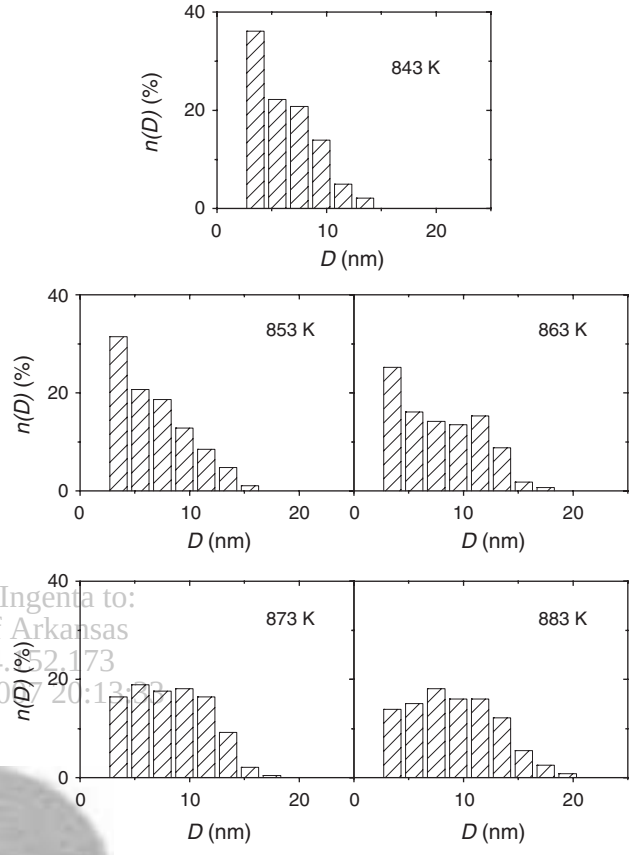

Fig. 11. Grain size distribution of nanocrystalline samples pre-heated up to different T_a.

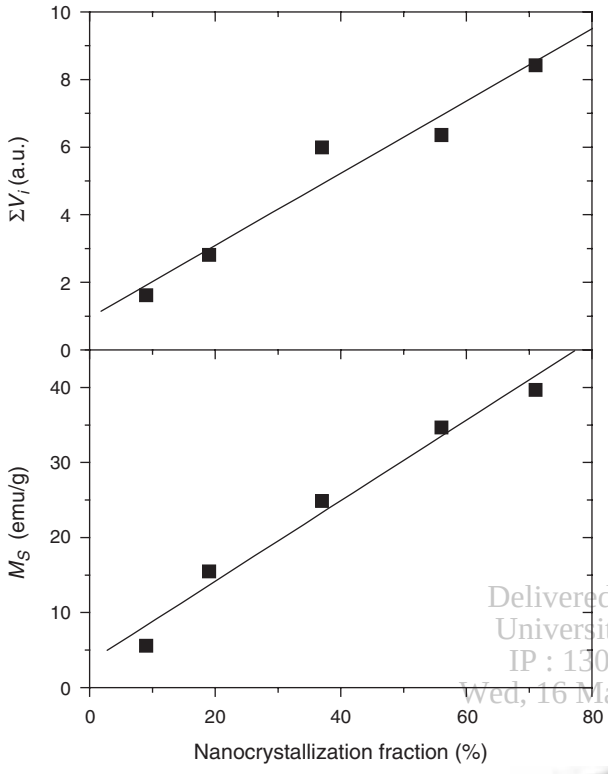

Fig. 12. Crystalline volume (from TEM) and saturation magnetization (from VSM) as a function of the completed fraction of the nanocrystallization process (from DSC), for samples pre-heated up to different T_a. Regression lines are plotted.

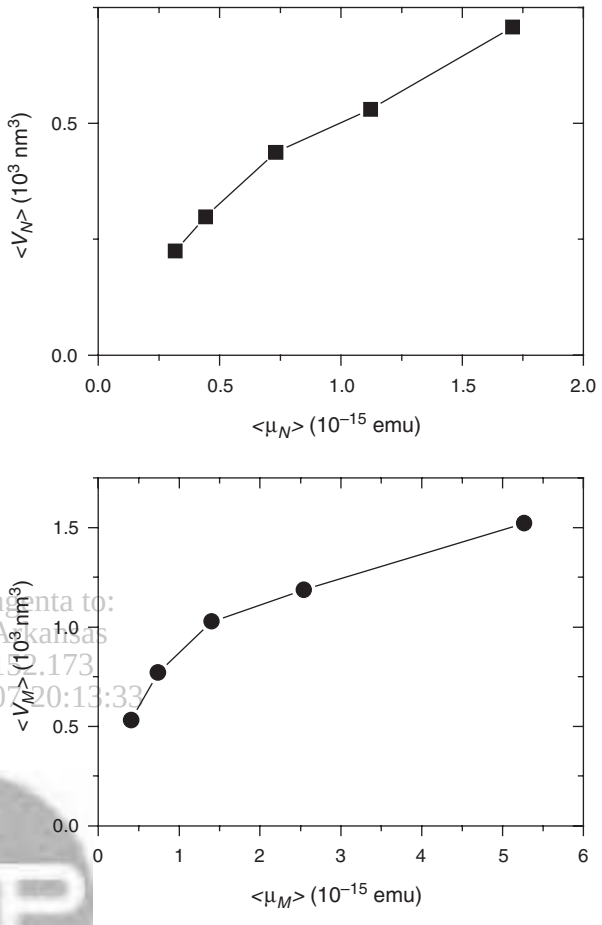

Fig. 13. Average particle volumes ($\langle V_M \rangle$ and $\langle V_N \rangle$) versus the corresponding average magnetic moment ($\langle \mu_M \rangle$ and $\langle \mu_N \rangle$, respectively). Lines are a guide to the eye.

Finally, in the case of VSM results, the saturation magnetization, M_S, can be considered proportional to the transformed fraction. The ratio between each couple of crystalline fractions obtained by these three experimental methods is a constant. The good linear correlation between TEM and VSM results with DSC results observed in Figure 12 supports the approximations stated above.

Whereas DSC results give information only about the total volume transformed, TEM and VSM techniques can supply average values of the volume and magnetic moment of the particles, respectively. For a single superparamagnetic particle, its magnetic moment, μ_i, is proportional to its volume, V_i. Therefore, it is possible to check this proportionality for the average values obtained from VSM and TEM results. The two possible values of $\langle \mu \rangle$ yield two mean values of $\langle V \rangle$:

$$\langle \mu_N \rangle = \frac{\sum N_i \mu_i}{\sum N_i} = \frac{\sum N_i C V_i}{\sum N_i} = C \frac{\sum N_i V_i}{\sum N_i} = C \langle V_N \rangle \quad (11)$$

and

$$\langle \mu_M \rangle = \frac{\sum N_i \mu_i^2}{\sum N_i \mu_i} = \frac{\sum N_i C^2 V_i^2}{\sum N_i C V_i} = C \frac{\sum N_i V_i^2}{\sum N_i V_i} = C \langle V_M \rangle \quad (12)$$

where $C = n_{\text{at}} \mu_{\text{at}}$ is a constant, n_{at} is the "average atom" number density in the α-Fe(Si) nanocrystals and μ_{at} its magnetic moment. The first average volume is simply the numerical average of the particle sizes, whereas for the second average volume, the particle volume is weighted with its number of atoms (proportional to the volume). Figure 13 shows the correlation between the mean magnetic moment and the mean particle volume using both possibilities. Linearity is better fulfilled in the case of $\langle V_N \rangle$ versus $\langle \mu_N \rangle$ than for $\langle V_M \rangle$ versus $\langle \mu_M \rangle$, in agreement with the magnetization results. Considering that the atomic density in the α-Fe lattice is 2 atoms per unit cell of volume a^3 ($a \sim 0.285$ nm is the lattice parameter), the atomic moment obtained from the constant C (Eq. (11)) and averaged over all the studied samples, $2.3 \pm 0.7\ \mu_B$, is of the order of the magnetic moment of Fe atoms in α-Fe. The large errors of the volume measured from TEM (for an error of the grain diameter of 1 nm, $\Delta V/V > 30\%$ for $D < 10$ nm) prevent a further discussion on this parameter.

It must be taken into account that the two contributions, μ_1 and μ_2 ($\mu_1 > \mu_2$), with which it was possible to fit the experimental $M(H)$ plots, are in fact average values of magnetic moments. TEM results clearly show that a continuous distribution of grain sizes exits and not only two values of D and, therefore, μ_1 represents an average for the bigger particles and μ_2 represents an average

for the smaller ones. The evolution of both distributions (from TEM and VSM results, respectively) with T_a qualitatively agrees (see Fig. 11 and Table I). The width of the distributions becomes broader as the nanocrystallization progresses and the particle density for low magnetic moment and small grain size is higher than for high magnetic moment and large grain size contributions.

Finally, it would be interesting to consider some effects which would affect the relation between TEM observations and VSM results. Whereas from TEM images we can directly observe a distribution of crystal sizes, $M(H)$ plots give us the global response of the system, from which the distribution information can be extracted after a fitting process. Besides, the magnetic and the TEM crystal size may differ due to some physical reasons. For example, the Fe atoms located at the surface of the nanocrystals will be affected by the high concentration of Nb atoms just outside the nanocrystals and, therefore, the magnetic moment of these Fe atoms might be smaller than the corresponding value of an Fe atom in the inner regions of the nanocrystals, yielding a fictitious decrease in the magnetic results with respect to the actual grain size. On the other hand, this effect can be partially compensated if the Fe atoms in the amorphous matrix close to the nanocrystals were polarized.[24]

4. CONCLUSIONS

Two different methods to calculate the mean magnetic moment of a distribution of superparamagnetic particles have been employed: either considering the number density of particles ($\langle \mu_N \rangle$) or considering their contribution to the magnetization of the system ($\langle \mu_M \rangle$). In order to select the most adequate mean magnetic moment, two different criteria have been proposed. The first one is to find the monodisperse system which better resembles the experimental magnetization curve of the polydisperse real system. The second criterion corresponds to identify an average magnetic energy which produces the collapse of the experimental magnetization curves after rescaling the x axis. With the help of numerical calculations, it has been shown that both criteria yield the same conclusions.

The selection of the most adequate mean magnetic moment depends on both the characteristics of the magnetic moment distribution and the range of the applied magnetic field. For broad distributions or low magnetic fields (well below saturation), $\langle \mu_M \rangle$ should be selected, while for narrow distributions and almost saturating magnetic fields, $\langle \mu_N \rangle$ gives a better description of the system.

Experimental results of superparamagnetic magnetization curves and grain size distribution from TEM have been obtained for nanocrystalline samples of a Mo-containing Finemet-type alloy. Applying the previously described selection criteria, the most adequate mean magnetic moments have been identified. These results are in agreement with the information extracted from the grain size distributions obtained from TEM.

Acknowledgments: This work was supported by the Spanish Government and EU-FEDER (Project MAT 2004-04618) and the PAI of Junta de Andalucía. J. S. B. is grateful to Junta de Andalucía for a research contract.

References and Notes

1. H. Gleiter, *Adv. Mater.* 4, 474 (**1992**).
2. M. E. McHenry, M. A. Willard, and D. E. Laughlin, *Prog. Mater. Sci.* 44, 291 (**1999**), and references therein.
3. A. Hernando, M. Vázquez, T. Kulik, and C. Prados, *Phys. Rev. B* 51, 3581 (**1995**).
4. A. Slawska-Waniewska, M. Gutowski, H. Lachowicz, T. Kulik, and H. Matyja, *Phys. Rev. B* 46, 14594 (**1992**).
5. V. Franco, C. F. Conde, A. Conde, and L. F. Kiss, *J. Magn. Magn. Mater.* 215, 400 (**2000**).
6. V. Franco, L. F. Kiss, T. Kemény, I. Vincze, C. F. Conde, and A. Conde, *Phys. Rev. B* 66, 224418 (**2002**).
7. V. Franco, C. F. Conde, A. Conde, and L. F. Kiss, *Phys. Rev. B* 72, 174424 (**2005**).
8. F. Sánchez-Bajo, A. L. Ortiz, and F. L. Cumbrera, *Acta Mater.* 54, 1 (**2006**).
9. P. Scardi and M. Leoni, *Acta Cryst.* A58, 190 (**2002**).
10. S. Calvin, S. X. Luo, C. Caragianis-Broadbridge, J. K. McGuiness, E. Anderson, A. Lehman, K. H. Wee, S. A. Morrison, and L. K. Kurihara, *Appl. Phys. Lett.* 87, 233102 (**2005**).
11. R. J. Marín-Palma, L. Pascual, P. Herrero, and J. M. Martínez-Duart, *Appl. Phys. Lett.* 87, 211906 (**2005**).
12. P. Allia, M. Coisson, M. Knobel, P. Tiberto, and F. Vinai, *Phys. Rev. B* 60, 12207 (**1999**).
13. P. Allia, F. Ghigo, M. Knobel, P. Tiberto, and F. Vinai, *J. Magn. Magn. Mater.* 158, 319 (**1996**).
14. H. K. Lachowicz, K. Zaveta, and A. Slawska-Waniewska, *IEEE Trans. Magn.* 38, 3033 (**2002**).
15. A. Kákay, M. Gutowski, L. Takács, V. Franco, and L. K. Varga, *J. Phys. A: Math. Gen.* 37, 6027 (**2004**).
16. T. Weser and K. Stierstadt, *Z. Phys. B* 59, 253 (**1985**).
17. L. Takacs, *J. Appl. Phys.* 63, 4264 (**1988**).
18. M. W. Gutowski, *J. Phys. A: Math. Gen.* 27, 7893 (**1994**).
19. V. Franco and A. Conde, *J. Magn. Magn. Mater.* 277, 181 (**2004**).
20. K. Yakushiji, S. Mitani, K. Takanashi, J. G. Ha, and H. Fujimori, *J. Magn. Magn. Mater.* 212, 75 (**2000**).
21. C. F. Conde, V. Franco, and A. Conde, *Phil. Mag. B* 76, 489 (**1997**).
22. K. Hono, *Prog. Mater. Sci.* 47, 621 (**2002**).
23. J. M. Barandiarán, I. Tellería, J. S. Garitaonandía, and H. A. Davies, *J. Non-Cryst. Solids* 329, 57 (**2003**).
24. A. Hernando, I. Navarro, and P. Gorria, *Phys. Rev. B* 51, 3281 (**1995**).

Received: 19 January 2006. Revised/Accepted: 28 August 2006.